Structural Engineering and Mechanics, Vol. 39, No. 6 (2011) 767-793
DOI: http://dx.doi.org/10.12989/sem.2011.39.6.767

An edge-based smoothed finite element method for adaptive analysis

L. Chen[2,3a], J. Zhang*[1], K.Y. Zeng[4b] and P.G. Jiao[5a]

[1] *Department of Civil and Environmental Engineering, National University of Singapore, 1 Engineering Drive 2, Singapore 117576*
[2] *Centre for Advanced Computations in Engineering Science (ACES), National University of Singapore, 9 Engineering Drive 1, Singapore 117576*
[3] *Institute of High Performance Computing, Singapore 138632*
[4] *Department of Mechanical Engineering, National University of Singapore, 9 Engineering Drive 1, Singapore 117576*
[5] *School of Mechanical Engineering, Shandong University, Jinan 250061, P.R. China*

(Received March 3, 2010, Accepted June 22, 2011)

Abstract. An efficient edge-based smoothed finite element method (ES-FEM) has been recently developed for solving solid mechanics problems. The ES-FEM uses triangular elements that can be generated easily for complicated domains. In this paper, the complexity study of the ES-FEM based on triangular elements is conducted in detail, which confirms the ES-FEM produces higher computational efficiency compared to the FEM. Therefore, the ES-FEM offers an excellent platform for adaptive analysis, and this paper presents an efficient adaptive procedure based on the ES-FEM. A smoothing domain based energy (SDE) error estimate is first devised making use of the features of the ES-FEM. The present error estimate differs from the conventional approaches and evaluates error based on smoothing domains used in the ES-FEM. A local refinement technique based on the Delaunay algorithm is then implemented to achieve high efficiency in the mesh refinement. In this refinement technique, each node is assigned a scaling factor to control the local nodal density, and refinement of the neighborhood of a node is accomplished simply by adjusting its scaling factor. Intensive numerical studies, including an actual engineering problem of an automobile part, show that the proposed adaptive procedure is effective and efficient in producing solutions of desired accuracy.

Keywords: smoothed finite element method (SFEM); edge-based smoothed finite element method (ES-FEM); complexity study; adaptive analysis; error estimate; local refinement

1. Introduction

Although the finite element method (FEM) (Zienkiewicz and Taylor 2000) has seen a great success in a broad range of applications, it still possesses some inherent shortcomings, such as the difficulties in the generation of quality quadrilateral elements for complicated domain and poor

*Corresponding author, Research Fellow, E-mail: zhangjian@nus.edu.sg
[a]Ph.D. Candidate
[b]Associate Professor

accuracy in stress distribution for triangular elements due to the "overly-stiff" behavior. To avoid the mesh-related difficulties, meshfree methods (Liu 2002) have been developed and some of which can provide solutions to overcome these shortcomings, such as the well-known element free Galerkin (EFG) method (Belytschko *et al.* 1994) and meshless local Petrov-Galerkin (MLPG) method (Atluri and Zhu 1998).

In the other front of development of numerical methods, the strain smoothing operation has been used in the nonlocal continuum mechanics (Eringen and Edelen 1972), the smoothed particle hydrodynamics (SPH) (Lucy 1977), in resolving the material instabilities (Chen *et al.* 2000) and spatial instability in nodal integrated meshfree methods (Chen *et al.* 2001). This technique has also applied to the natural element method (Yoo *et al.* 2004). Recently, a smoothed finite element method (SFEM) has been developed by applying the strain smoothing technique to the FEM settings to overcome some of shortcomings in the FEM without too much increase in computational efforts (Liu *et al.* 2007). In the SFEM, cell-based strain smoothing technique is proposed in the conventional FEM formulation, so as to reduce the over stiffness of the FEM model. To further reduce the stiffness, a node-based smoothed finite element (NS-FEM) (Liu *et al.* 2009) has been formulated using the smoothing domains associated with the nodes. The NS-FEM works for triangular, 4-node quadrilateral and even n-sided polygonal elements. When triangular elements are used, the NS-FEM gives the same results as the node-based uniform strain elements (Dohrmann *et al.* 2000) or as the LC-PIM (known also as NS-PIM) (Liu and Zhang 2005) when the linear shape functions are used for interpolation. The NS-FEM, however, behaves "overly-soft" observed as non-zero energy spurious modes that can lead to temporal instability when it is used to solve the dynamic problems. To reduce this overly-soft behavior, an edge-based smoothed finite element (ES-FEM) was thus invented for both 2D (Liu *et al.* 2008) and 3D problems (Nguyen-Thoi *et al.* 2009). The ES-FEM uses the triangular mesh that can be generated automatically for problems with complicated geometry, and the strain smoothing domains are associated with the edges of elements. The ES-FEM can properly reduce the softening effects and gives a close-to-exact stiffness, and thus often exhibits super convergence properties, ultra accuracy and high computational efficiency compared to the traditional FEM using the same meshes. Because of these excellent features, the ES-FEM is found so far the best candidate for adaptive analysis.

In an adaptive analysis, there are essentially two major issues – error estimation and mesh refinement. The first requires a *posteriori* error estimate to measure the local and global errors in the solution obtained based on the current mesh, whereby a decision can be made to determine whether a refinement is required and if true, where to refine. The second decides how to perform the refinement based on the error information provided by the error estimate. The effectiveness and efficiency of these two operations are critical to the performance of an adaptive procedure. To conduct *a posteriori* error estimation for a field variable, two values of the variable– a computed value and a reference value – are required. The first is the raw value given by direct computations while the second is derived from the first via a post-processing (e.g., smoothing or projection). In the FEM model, the raw stresses do not possess inter-element continuity and have a low accuracy along element interfaces; the "improved" values are obtained via smoothing over the inter-element discontinuity. The difference between the raw and improved values provides a basis for error estimation in FEM. Detailed descriptions of this approach are referred to FEM literatures, e.g., by Zienkiewicz and Zhu (1987). In the context of adaptive FEM, Choi and Chung (1995) investigated the adaptive finite element control of spatial and temporal discretization errors for dynamic analysis. Ozakca (2003) performed adaptive finite element analysis of linear elastic problems using different error estimators. There are also some other methods (Kee *et al.* 2008, Zhang *et al.* 2008, Zhang and Liu 2008, Lee *et al.* 1998) used for error estimation and adaptive meshing in FEM or meshfree methods. As the stress field generated by ES-FEM is already very smooth on the element interfaces and the traditional error estimates based on stress smoothing techniques used in the FEM are no longer applicable, there is a need to develop different error estimates for adaptive analysis using the ES-FEM.

In general, the refinement can be classified into two categories: *h*-type refinement and *p*-type refinement (Zienkiewicz and Taylor 2000). The first one is the simple reduction of the element size, which is a popular way for most engineering problems with complicated geometries; the latter increases the order of polynomial approximation in the predefined elements. In this paper, a local refinement technique of *h*-type based on the Delaunay algorithm is implemented to achieve high efficiency. In this technique, each node is assigned a scaling factor to control local nodal density; refinement of the neighborhood of a node is accomplished simply by adjusting its scaling factor.

This paper presents an efficient adaptive procedure based on triangular elements using the ES-FEM. The procedure composes a smoothing domain based energy error (SDE) estimate and a local domain refinement technique. The paper is organized as follows. Section 2 provides a brief description of ES-FEM. Section 3 describes the overall flow of the present adaptive procedure. In Section 4, the smoothing domain based energy error estimate is elaborated and tested. Section 5 focuses on the development of a local technique for domain refinement. Section 6 presents some numerical applications. The paper concludes with a review of the proposed techniques in the Section 7.

2. Briefing on the ES-FEM

2.1 Governing equations

Consider a 2D static elastic problem governed by the equilibrium equation in the domain Ω bounded by $\Gamma(\Gamma = \Gamma_u + \Gamma_t;\ \Gamma_u \cap \Gamma_t = 0)$ as

$$\nabla \cdot \boldsymbol{\sigma} + \mathbf{b} = 0 \quad \text{in} \quad \Omega \tag{1}$$

where ∇ is the divergence operator, $\boldsymbol{\sigma}$ is the Cauchy stress tensor and $\mathbf{b}$ is the body force term.

The essential and natural boundary conditions are given by

$$\mathbf{u} = \mathbf{u}_\Gamma \quad \text{on} \quad \Gamma_u \tag{2}$$

$$\boldsymbol{\sigma} \cdot \mathbf{n} = \mathbf{t}_\Gamma \quad \text{on} \quad \Gamma_t \tag{3}$$

where $\mathbf{u}_\Gamma$ and $\mathbf{t}_\Gamma$ are the vectors of the prescribed displacements and tractions respectively, and $\mathbf{n}$ is the outward normal unit vector defined on the boundary Γ.

The constitution equation (stress-strain relation) is given by

$$\boldsymbol{\sigma} = \mathbf{D}\boldsymbol{\varepsilon} \tag{4}$$

where $\mathbf{D}$ is the matrix of material constants, and $\boldsymbol{\sigma}^T = \{\sigma_{xx}\ \ \sigma_{yy}\ \ \tau_{xy}\}$ and $\boldsymbol{\varepsilon}^T = \{\varepsilon_{xx}\ \ \varepsilon_{yy}\ \gamma_{xy}\}$ are the vector forms of the stress and strain tensor respectively.

The compatibility equation (strain-displacement relation) is given by

$$\boldsymbol{\varepsilon} = \nabla_s \mathbf{u} \tag{5}$$

where $\mathbf{u} = \{u_x \;\; u_y\}^T$ is the vector of the displacement and $\nabla_s \mathbf{u}$ is the symmetric gradient of the displacement field.

2.2 Edge-based strain smoothing

In the ES-FEM, however, we do not use the compatible strains $\boldsymbol{\varepsilon} = \nabla_s \mathbf{u}$ but the strains "smoothed" over the local smoothing domains. These local smoothing domains are constructed with respect to the edges of triangular elements such that $\Omega = \bigcup_{k=1}^{N_s} \Omega^{(k)}$ and $\Omega^{(i)} \cap \Omega^{(j)} = \varnothing$, $i \neq j$, in which N_s is the number of smoothing domains. For example, the smoothing domain corresponding to the inner edge k, $\Omega^{(k)}$, is formed by connecting two end points of edge k and two centroids of the adjacent triangular elements. The smoothing domain for the boundary edge m $\Omega^{(m)}$, is just one third region of triangular element which contains the edge m as shown in Fig. 1.

Using the edge-based smoothing domains, *smoothed* strains can be obtained using the *compatible* strains $\boldsymbol{\varepsilon} = \nabla_s \mathbf{u}$ through the following smoothing operation over domain $\Omega^{(k)}$ associated with the edge k

$$\hat{\boldsymbol{\varepsilon}}_k = \frac{1}{A^{(k)}} \int_{\Omega^{(k)}} \nabla_s \mathbf{u}(\mathbf{x}) d\Omega = \frac{1}{A^{(k)}} \int_{\Gamma^{(k)}} \mathbf{L}_n \mathbf{u}(\mathbf{x}) d\Gamma \tag{6}$$

where $A^{(k)} = \int_{\Omega^{(k)}} d\Omega$ is the area of the smoothing domain $\Omega^{(k)}$, $\Gamma^{(k)}$ is the boundary of the smoothing domain and $\mathbf{L}_n$ is the outward unit normal matrix which can be expressed as

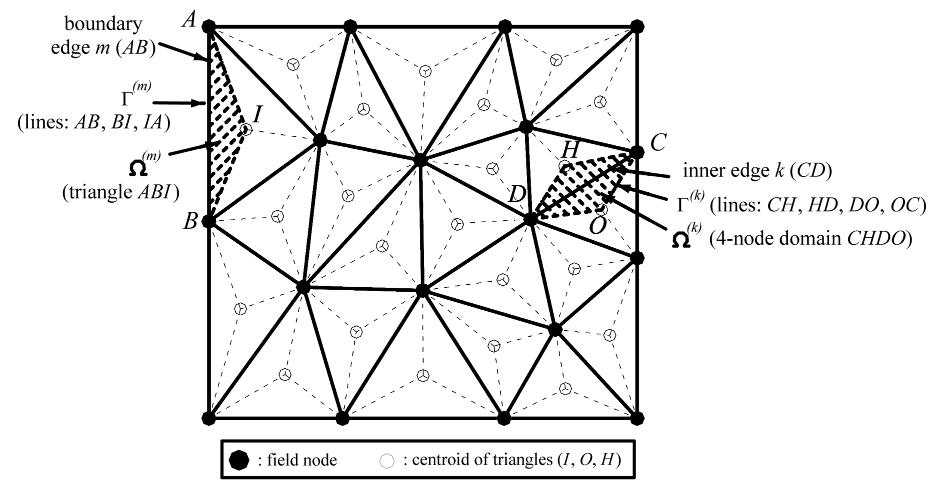

Fig. 1 A mesh of triangular elements and the smoothing domains associated with edges

$$\mathbf{L}_n = \begin{bmatrix} n_x & 0 \\ 0 & n_y \\ n_y & n_x \end{bmatrix} \tag{7}$$

The displacements within an element can be interpolated as

$$\mathbf{u} = \sum_{i=1}^{NP} \mathbf{N}_i \mathbf{d}_i \tag{8}$$

where NP is the number of the nodal variables of the element, $\mathbf{d}_i = [u_i \;\; v_i]^T$ is the nodal displacement vector.

Substituting Eq. (8) into Eq. (6), the smoothed strain can be written in the following matrix form of nodal displacements

$$\hat{\boldsymbol{\varepsilon}}_k = \sum_{i \in N_{infl}} \hat{\mathbf{B}}_i(\mathbf{x}_k)\mathbf{d}_i \tag{9}$$

where N_{infl} is the number of nodes in the influence domain of $\Omega^{(k)}$. In Eq. (9), the $\hat{\mathbf{B}}_i(\mathbf{x}_k)$ is termed as the smoothed strain matrix that can be calculated by

$$\hat{\mathbf{B}}_i(\mathbf{x}_k) = \begin{bmatrix} \hat{b}_{ix}(\mathbf{x}_k) & 0 \\ 0 & \hat{b}_{iy}(\mathbf{x}_k) \\ \hat{b}_{iy}(\mathbf{x}_k) & \hat{b}_{ix}(\mathbf{x}_k) \end{bmatrix} \tag{10}$$

Using the Gauss integration along each segment of boundary $\Gamma^{(k)}$, we have

$$\hat{b}_{ih} = \frac{1}{A^{(k)}} \sum_{m=1}^{N_{seg}} \left[\sum_{n=1}^{N_{gau}} w_n N_i(\mathbf{x}_{mm}) n_h(\mathbf{x}_m) l_m^{(k)} \right] \quad (h = x, y) \tag{11}$$

where N_{seg} is the number of segments of the boundary $\Gamma^{(k)}$, N_{gau} is the number of Gauss points used in each segment, w_n is the corresponding weight of Gauss points, n_h is the outward unit normal corresponding to each segment on the smoothing domain boundary and $l_m^{(k)}$ is the length of the m-th segment in smoothing domain $\Omega^{(k)}$.

2.3 Discretized system equation

The discrete equations of ES-FEM are generated from the smoothed Galerkin weak form

$$\int_\Omega \delta(\hat{\varepsilon}(\mathbf{u}))^T \mathbf{D}(\hat{\varepsilon}(\mathbf{u})) d\Omega - \int_\Omega \delta\mathbf{u}^T \mathbf{b} d\Omega - \int_{\Gamma_t} \delta\mathbf{u}^T \mathbf{t}_\Gamma d\Gamma = 0 \tag{12}$$

Substituting the approximated displacements in Eq. (8) and the smoothed strains from Eq. (6) into the smoothed Galerkin weak form, and invoking the arbitrary nature of the variation operations, a set of discretized algebraic system equations can be obtained in the following matrix form

$$\widehat{\mathbf{K}}\mathbf{d} = \mathbf{f} \tag{13}$$

where $\mathbf{d}$ is the displacement vector of all the nodes, $\widehat{\mathbf{K}}$ is the global stiffness matrix and $\mathbf{f}$ is the nodal force vector that can be obtained by

$$\mathbf{f} = \int_{\Omega} N^T(\mathbf{x})\mathbf{b}d\Omega + \int_{\Gamma_t} N^T(\mathbf{x})\mathbf{t}_{\Gamma}d\Gamma \tag{14}$$

The entries in sub-matrices of the stiffness matrix $\widehat{\mathbf{K}}$ in Eq. (13) can then be expressed as

$$\widehat{\mathbf{K}}_{ij} = \sum_{k=1}^{N_s} \widehat{\mathbf{K}}_{ij}^{(k)} \tag{15}$$

where the summation means an assembly process, and $\widehat{\mathbf{K}}_{ij}^{(k)}$ is the stiffness matrix associated with the smoothing domain $\Omega^{(k)}$ and can be computed by

$$\widehat{\mathbf{K}}_{ij}^{(k)} = \int_{\Omega^{(k)}} \widehat{\mathbf{B}}_i^T \mathbf{D} \widehat{\mathbf{B}}_j d\Omega = \widehat{\mathbf{B}}_i^T \mathbf{D} \widehat{\mathbf{B}}_j A^{(k)} \tag{16}$$

where the strain gradient matrix $\widehat{\mathbf{B}}_i$ is computed by Eq. (11).

2.4 Efficiency of the ES-FEM solver

In general, the computational cost is mainly to solve the final discrete system equations, which depends on the square of bandwidth w of the global stiffness matrix ($\frac{1}{2}N_{node}w^2$). The global stiffness matrix $\widehat{\mathbf{K}}$ of the ES-FEM and the NS-FEM has the same dimension as that of FEM using the same mesh. In the FEM, the bandwidth of $\widehat{\mathbf{K}}$ depends on the largest difference of nodal sequence number of the elements. In detail, a sample node influences the bandwidth of stiffness matrix by the difference between the sample node and its interrelated nodes during the assembling process. These interrelated nodes are called the *bandwidth influence node group* here. Since the basic unit for assembling is the element, the nodes involved in the surrounding elements of the sample node form its *bandwidth influence node group*. Most importantly, the bandwidth is really controlled by the nodal sequence number difference between the sample node and the node with the smallest sequence number in its *bandwidth influence node group*. Here, we can call this difference as the *influence difference* and the assembling unit containing the node with the smallest sequence number as the *influence assembling unit*. For example, as shown in Fig. 2(a), the *influence assembling unit* is the triangle with shadow, and the *influence difference* of the sample node 22 is the sequence number difference between itself and the node 5, i.e., $22 - 5 = 17$. In practice, renumbering nodes are often used to reduce the bandwidth and the computation cost (Liu 2002). The nodal sequence number is sorted along one dimension after renumbering as shown in Fig. 2(b). The sample node 22 is changed to node 15, and the *influence assembling unit* (the triangle with shadow) is located at the lower left side of the sample node. Clearly, the corresponding *influence difference* is reduced to $15 - 8 = 7$. This means that the bandwidth will be reduced significantly. Note that the *influence difference* is close to the number of nodes along the sorted dimension. This is because the *influence assembling unit* is just across one level of the elements.

The similar renumbering operation is performed in the ES-FEM and NS-FEM. The smoothing

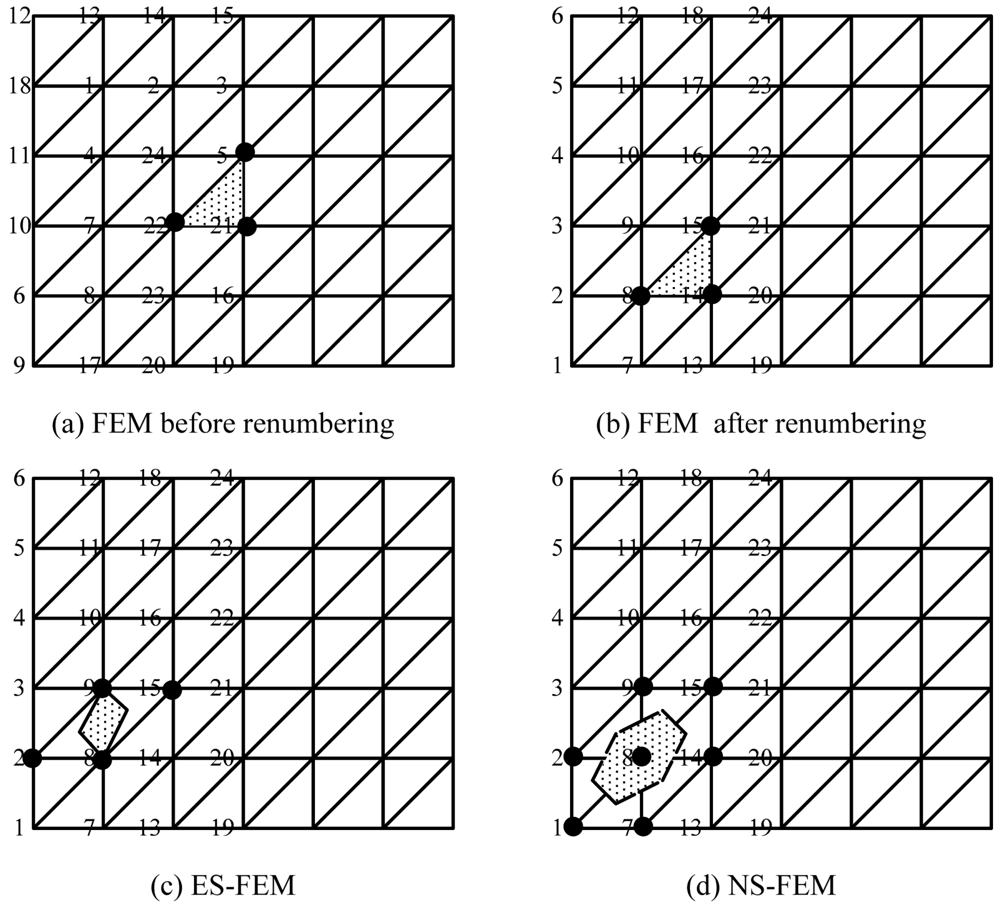

Fig. 2 Illustration of the bandwidth

Table 1 Comparison of computation time using different numerical methods with triangular elements*

Nodes	Elements	ES-FEM	NS-FEM	FEM
2192	4142	0.172 s	0.313 s	0.079 s
9376	18270	3.407 s	4.812 s	1.329 s
16010	31218	8.609 s	12.39 s	3.338 s
44407	87612	70.97 s	95.68 s	20.562 s

*Tests were conducted for the cantilever problem on a Dell PC of Intel® Pentium(R) CPU 2.80GHz, 1.00GB of RAM.

domains associated with nodes or edges are the basic unit for assembling the stiffness matrix $\widehat{\mathbf{K}}$. Hence, the largest difference of nodal sequence number associated with the smoothing domains influences the bandwidth. Since the smoothing domains associated with nodes and edges are generally across two levels of elements, the *influence difference* of ES-FEM and NS-FEM almost equals to twice more than the number of nodes along the sorted dimension, which also is the

Table 2 Computational efficiency: CPU time (s) needed for obtaining the results of the same accuracy in displacement norm (for error in solutions at e_d = 1.0e-004)

Methods	FEM	ES-PIM	NS-PIM
Solver time	92.358	11.09	270.59
Efficiency Ratio*	1	8.3283	0.34132

*Computational efficiency is inverse proportion to CPU time.

influence difference of FEM. For example, the *influence difference* of ES-FEM and NS-FEM is, respectively, $15-2 = 13$ and $15-1 = 14$ as illustrated in Figs. 2(c)-(d).

Table 1 lists the computation time using the ES-FEM, NS-FEM, and FEM tested on a cantilever example. The comparison is performed on the same DELL PC of Intel® Pentium(R) CPU 2.80GHz, 1.00GB of RAM. It can be clearly seen that the computation time of ES-FEM and NS-FEM is about 2-5 times more than that of FEM. As the bandwidth analysis above, the bandwidth (i.e., *influence difference*) of ES-FEM and NS-FEM is almost twice more than that of FEM. Therefore, the computation time is nearly 4 times more than that of FEM, which is in good agreement with the test results.

Note that the solution accuracy of ES-FEM using triangular elements is much better than FEM using the same mesh. Therefore, in terms of computational efficiency (computation time for the same accuracy), the ES-FEM has been found superior to FEM. To investigate quantitatively the numerical results, the error in displacement are defined as follows

$$e_d = \sqrt{\frac{\sum_{i=1}^{n}(u_i^{exact} - u_i^{numerical})^2}{\sum_{i=1}^{n}(u_i^{exact})^2}} \tag{17}$$

where the superscript *exact* denotes the exact or analytical solution, numerical denotes numerical solution obtained using a numerical method, and A is the area of the problem domain.

The computational efficiency in terms of CPU time (s) needed for obtaining the results of the same accuracy in displacement norm (for error in solutions at e_d = 1.0e-004) is compared in Table 2. The FEM serves as the “bottom point”. We can clearly see that the efficiency ratio of ES-FEM with a value of 8.33 is the largest with respect to the FEM and the NS-FEM. Therefore, The ES-FEM is confirmed in this study as the preferred solver for our adaptive analysis.

3. Adaptive procedure

Adaptive procedures require a refinement criterion for local mesh enrichment and a stop criterion for termination of procedure (Chung and Belytschko 1998). First, to determine where to refine and leave most of mesh configuration unchanged, the approximation error needs to be estimated locally and a refinement criterion needs to be predefined. At the same time, to access whether solution reaches to a desired accuracy, a stop criterion is also required.

Fig. 3 presents the basic flow chart for each adaptive procedure using the ES-FEM, in which, $R_{threshold}$ is the predefined threshold relative nodal error and $\eta_{threshold}$ the allowable relative global

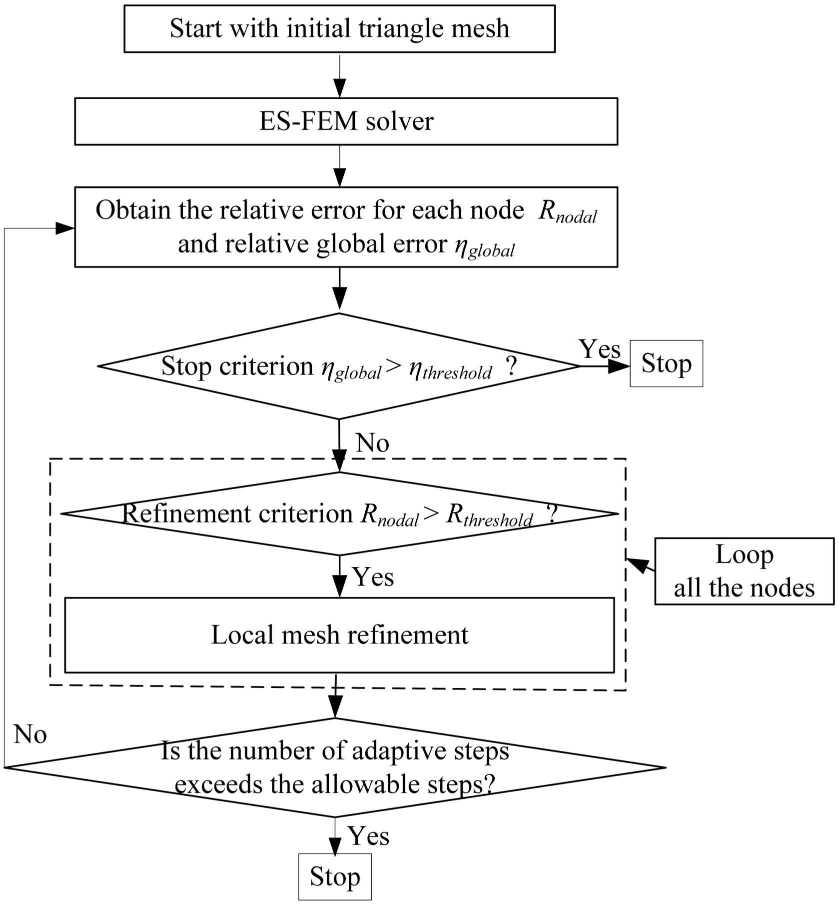

Fig. 3 Flow chart of the adaptive procedure using the ES-FEM. $R_{threshold}$ is defined as the threshold relative nodal error and $\eta_{threshold}$ the allowable relative global error estimation

error estimation. First, triangular elements are created using the Delaunay technique and the solutions of stress are computed using the ES-FEM. The second step is to calculate the relative error R_{nodal} for each node and relative global error estimation η_{global} using a smoothing domain based energy (SDE) error estimate, which will be further discussed in section 5. Third, the comparison of η_{global} and $\eta_{threshold}$ determines whether or not to stop the adaptive procedure. Fourth, the local refinement is performed when $R_{nodal} > R_{threshold}$. Finally, a check on whether the number of adaptive steps exceeds the predefined maximum adaptive steps is conducted, and if true, the adaptive procedure exits.

4. Smoothing domain based energy (SDE) error estimation

As mentioned earlier, error estimates for FEM are not applicable to error analysis in the ES-FEM, and proper approaches must be devised. In the existing literatures, error estimates are generally classified into two major types: recovery based and residual based error estimates. The recovery based error estimate is first introduced by Zienkiewicz and Zhu (1987). This error estimate is obtained through the recovery processes upon the raw data obtained from the FEM model and is expressed in terms of the strain energy norm. The residual based error estimates were proposed by Babuska and Rheinboldt (1978) and recently were applied to the meshfree context by Kee *et al.* (2008) and Zhang *et al.* (2008). This paper develops an efficient and effective *a posteriori* error estimate that works well for the ES-FEM settings. Two important features of ES-FEM that concerns the error estimate are: (1) the strain or stress is constant in a smoothing domain associated with edges of elements; (2) the domain integration in ES-FEM is also based on these smoothing domains. Therefore, the proposed (SDE) error estimate examines energy error in each triangular element using the strains of the smoothing domains hosted by the element and uses it as an indication of errors.

An error estimate for an approximation is usually constructed based on the difference between the approximate and exact solutions. For a quantity $\mathbf{q}$ defined over domain Ω and its approximation $\hat{\mathbf{q}}$, a general measure of the approximation error e has the form of

$$e = L(\mathbf{q}, \hat{\mathbf{q}}) \tag{18}$$

where L denotes an norm measure (e.g., L_1 norm, L_2 norm, energy etc.) In most problems, $\mathbf{q}$ in exact form is not available and hence a reference value derived from $\hat{\mathbf{q}}$ is used. In solid mechanics, the quantity can be displacement, strain, stress or energy.

A conventional implementation of Eq. (18) is to use the L_2 norm error, i.e.

$$e_{L_2} = \|\mathbf{q}(x) - \hat{\mathbf{q}}(x)\|_{L_2} = (\mathbf{q}(x) - \hat{\mathbf{q}}(x))^T \cdot (\mathbf{q}(x) - \hat{\mathbf{q}}(x))^{1/2} \tag{19}$$

When $\mathbf{q}$ is the stress or strain, and integral measure is adopted, the energy norm over domain Ω can be written as

$$\|e\|_\Omega = \left(\int_\Omega (\boldsymbol{\varepsilon} - \hat{\boldsymbol{\varepsilon}})^T \mathbf{D} (\boldsymbol{\varepsilon} - \hat{\boldsymbol{\varepsilon}}) d\Omega\right)^{1/2} \tag{20}$$

where $\boldsymbol{\varepsilon}$ are strain in the domain Ω.

In an ES-FEM model, two kinds of domains are used: triangle element domain Ω_e and smoothing domain Ω_s as shown in Fig. 4. Each triangular element hosts three parts of smoothing domains associated with three edges of the elements, e.g., element Ω_s hosts $\Omega_s^{(1)}, \Omega_s^{(2)}$ and $\Omega_s^{(3)}$ are involved. Since the strains and stresses are constant in each of these three smoothing domains, the energy error in a triangular element is thus estimated as

$$\|e\|_\Omega = ((\Delta\boldsymbol{\varepsilon}_{\max})^T \mathbf{D} (\Delta\boldsymbol{\varepsilon}_{\max}) \times A)^{1/2} \tag{21}$$

where A is the triangular element area and $\Delta\boldsymbol{\varepsilon}_{\max}$ the maximum difference of strain between the three smoothing domains, which can be described

$$\Delta\boldsymbol{\varepsilon}_{\max} = \max(|\boldsymbol{\varepsilon}^{(1)} - \boldsymbol{\varepsilon}^{(2)}|, |\boldsymbol{\varepsilon}^{(2)} - \boldsymbol{\varepsilon}^{(3)}|, |\boldsymbol{\varepsilon}^{(3)} - \boldsymbol{\varepsilon}^{(1)}|) \tag{22}$$

It is clear From Eq. (21) that the energy error in a triangular element is defined as the strain energy of maximum difference of strain among three smoothing domains associated with these three edges of the element. Therefore, the estimated energy error in a triangular element is a little larger than the exact energy error. However, the high error region can be well captured, which is important for our adaptive analysis.

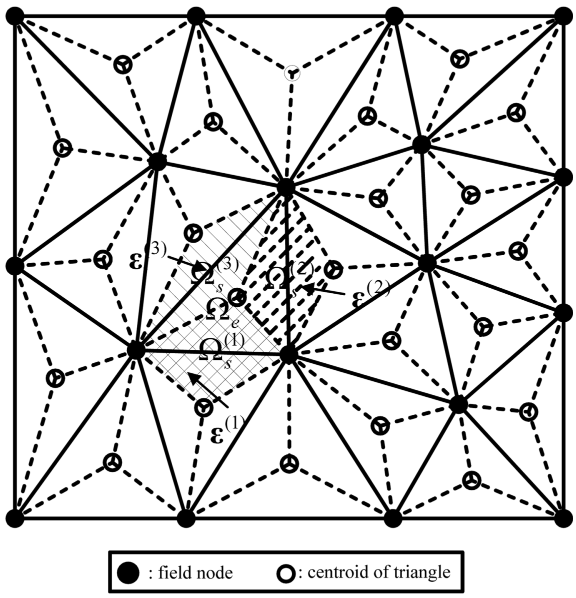

Fig. 4 Triangular element energy error estimate based on smoothing domains associated with edges of elements. For the triangular element Ω_e, smoothing domains $\Omega_s^{(1)}$, $\Omega_s^{(2)}$ and $\Omega_s^{(3)}$ are involved

5. Strategy for local adaptive refinement

In adaptive analysis, the problem domain needs to be refined automatically without human intervention until the desired accuracy is achieved or the maximum allowable number of iterations is exceeded. It is usually undesirable to refine the entire domain at each iteration, as in many cases only a few locations exhibit poor approximations. To achieve high efficiency, it is therefore preferred to focus only on these locations. The present local refinement approach is developed with this consideration. It is based on triangular elements for easy automated refinement and uses a local Delaunay algorithm to perform the refinement with the aid of scaling factors. A detailed description of this strategy is given in the following.

5.1 Integration based on triangular mesh

Since the ES-FEM works perfectly well for triangular elements, the present implementation uses the triangular mesh with the vertices of triangular elements coinciding with the field nodes. This brings much ease and flexibility for automatic mesh generation for domain of arbitrary shape. The present study first devises an automatic mesh generator using the Delaunay triangulation technique (Liu and Tu 2002), which can be employed to perform triangulation for either global or local domain, as desired.

In the process of triangulation, a scaling factor is assigned to each node to reflect local nodal density; it is evaluated from the surrounding element area using

$$S_{nodal} = \sqrt{\frac{2}{m_e}\sum_{i=1}^{m_e} A_e^{(i)}} \tag{23}$$

where S_{nodal} is the scaling factor of node, m_e the number of surrounding elements, and $A_e^{(i)}$ the area of the i-th surrounding element. The scaling factor is an index of local nodal distance and plays an important role in the later local refinement procedure.

5.2 Update of scaling factor

The scaling factor at a node will be updated if refinement is required at its location. The change of scaling factor is based on the distribution of local error measured by the smoothing domain based energy (SDE) error estimate. This is done by converting element energy error to nodal energy error: the former is equally distributed to element vertices and the latter is an accumulation of contributions from surrounding elements, i.e.

$$\|e_{nodal}\| = \sqrt{\sum_{i=1}^{m_e} \frac{\|e^{(i)}\|^2}{n}} \tag{24}$$

where n the number of element vertices (n = 3 for a triangular element), and $\|e^{(i)}\|$ the energy error of the i-th surrounding element, which can be obtained using Eq. (21). A relative error measure is then defined for each node

$$R_{nodal} = \sqrt{\frac{\|e_{nodal}\|^2}{E_{nodal}}} \tag{25}$$

where R_{nodal} is the nodal relative error, and E_{nodal} the nodal energy converted from the smoothing domain energy

$$E_{nodal} = \sum_{i=1}^{m_s} \frac{(\boldsymbol{\sigma}^{(i)})^T(\boldsymbol{\varepsilon}^{(i)})}{4} \times A_s^i = \sum_{i=1}^{m_s} \frac{(\boldsymbol{\varepsilon}^{(i)})^T \mathbf{D}(\boldsymbol{\varepsilon}^{(i)})}{4} \times A_s^i \tag{26}$$

where m_s is the number of smoothing domains associated with a node, and $\boldsymbol{\sigma}^{(i)}$, $\boldsymbol{\varepsilon}^{(i)}$ and $A_s^{(i)}$ are the stress, strain and area of the i-th surrounding smoothing domain respectively.

To determine the locations where refinement is required, the nodes are first heap sorted by nodal relative error; a threshold nodal relative error is then obtained based on the predefined mesh refinement percentage (α%) and the relative error at each node is compared with this value. If the threshold value is exceeded, the scaling factor at a node will be changed to

$$S_{nodal}^* = \frac{R_{threshold}}{R_{nodal}} S_{nodal} \tag{27}$$

$$R_{threshold} = R_{nodal}^{N_n \times \alpha\% - 1} \tag{28}$$

where S_{nodal} and S_{nodal}^* are the old and new values of a scaling factor, respectively, and $R_{nodal}^{N_n \times \alpha\% - 1}$ is the relative error of node with a index of $N_n \times \alpha\% - 1$ after the heap sorting, in which N_n is the total number of nodes in global domain. After the change of a scaling factor is made, a local Delaunay algorithm will be executed.

5.3 Local Delaunay triangulation

The Delaunay triangulation technique can be applied to an arbitrary 2-D domain. Given a set of

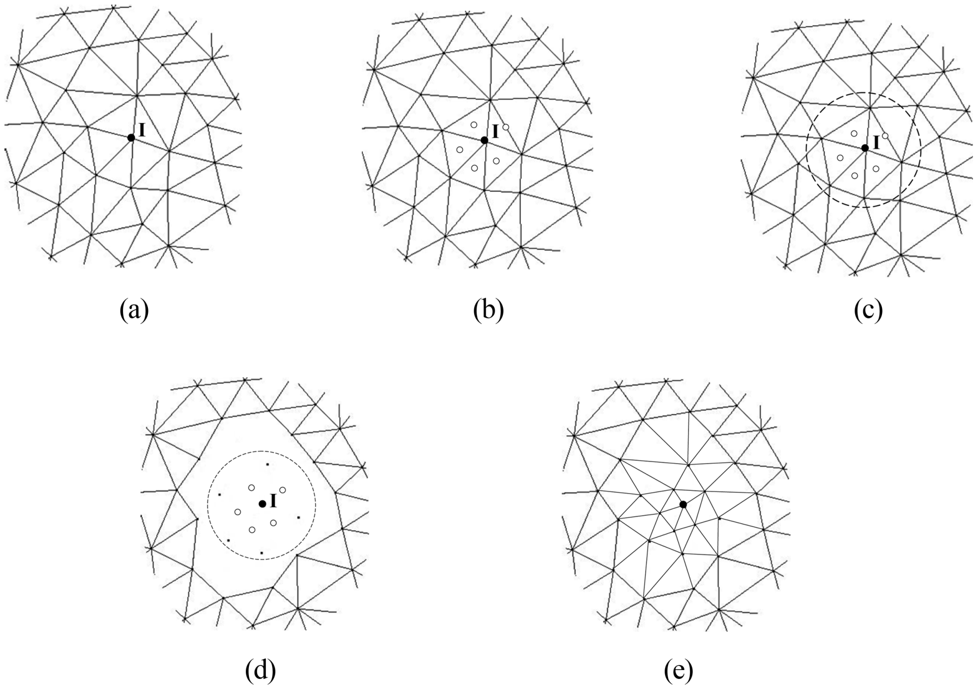

Fig. 5 Stages in the local domain refinement (a) original mesh, (b) insertion of nodes, (c)-(d) formulation of a local block and (e) refined mesh

nodes and a discretized boundary that encloses the nodes, the technique can generate an optimal triangular mesh for the bounded domain based on the existing nodes. This versatility enables a local domain to be refined easily and forms the basis of the present approach. To illustrate this, consider an example depicted in Fig. 5(a), where the scaling factor of node I is changed from S_I to S_I^* ($S_I^* < S_I$). The procedures for local refinement comprise:

(1) Insertion of nodes. New nodes are inserted by looping the surrounding triangles: for an acute triangle a node is inserted at the center of its circumcircle while for an obtuse triangle, a new node is introduced at the middle of the longest edge (Fig. 5(b)).

(2) Formulation of local domain. This is done by drawing a circle centered at node I (Fig. 5(c)) and then removing all element edges inside or intersecting the circle (Fig. 5(d)). The circle radius dictates the block size and is used to control the range of mesh revision.

(3) Triangulation of the local domain using the Delaunay algorithm. This regenerates a triangular mesh for the local domain based on the existing nodes inside the block (Fig. 5(e)).

(4) Recalculation of scaling factors. Scaling factors for all affected nodes are updated based on the new mesh.

The refinement procedures will be repeated if the updated scaling factor of node I is still larger than S_I^*. This local refinement approach is very efficient, especially for problems with a large number of nodes. Other variants of this strategy may be devised. In an iterative solution procedure, the variables at new nodes are evaluated based on the old nodes, thus providing a starting solution for next iteration.

5.4 Stop criterion of adaptive refinement

The adaptive refinement stops automatically when the relative global error η_{global} is more than the allowable value $\eta_{threshold}$

$$\eta_{global} = \sqrt{\|e_{global}\|^2 / E_{global}} > \eta_{threshold} \tag{29}$$

where e_{global} is the summation of energy error over all triangular elements yields the global error, and E_{global} the global strain energy in the whole domain, which can be given as

$$\|e_{global}\| = \sqrt{\sum_{i=1}^{N_e} \|e^{(i)}\|^2} \tag{30}$$

where N_e is the total number of triangular elements and $\|e^{(i)}\|$ the energy error (using Eq. (21)) of the i-th element.

$$E_{global} = \sum_{i=1}^{N_s} \frac{(\boldsymbol{\sigma}^{(i)})^T (\boldsymbol{\varepsilon}^{(i)})}{2} \times A_s^{(i)} = \sum_{i=1}^{N_s} \frac{(\boldsymbol{\varepsilon}^{(i)})^T \mathbf{D} (\boldsymbol{\varepsilon}^{(i)})}{2} \times A_s^{(i)} \tag{31}$$

where N_s is the total number of smoothing domain, and $\boldsymbol{\sigma}^{(i)}, \boldsymbol{\varepsilon}^{(i)}$ and $A_s^{(i)}$ are the strain, stress and area of the i-th smoothing domain in the whole domain respectively.

6. Numerical experiments

6.1 Examination of the SDE error estimation

The validation of the smoothing domain based energy (SDE) error estimate is conducted with three elastostatic problems of plane stress conditions. The first is a cantilever subjected to a load at the free end as shown in Fig. 6. The second is an infinite plate with a circular hole subjected to a unit tensile traction in the horizontal direction as shown in Fig. 7. The third is an infinite square plate containing a crack subjected to boundary conditions prescribed by the near crack-tip field solution as shown in Fig. 8. The material properties are Young's modulus $E = 3.0 \times 10^7$ and Poisson's ratio $\nu = 0.3$. All the three problems have analytical solutions and therefore quantitative verification can be made. The "exact" energy is computed based on the analytical solutions.

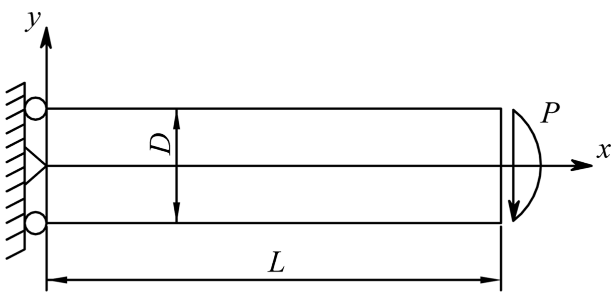

Fig. 6 Cantilever loaded at the end

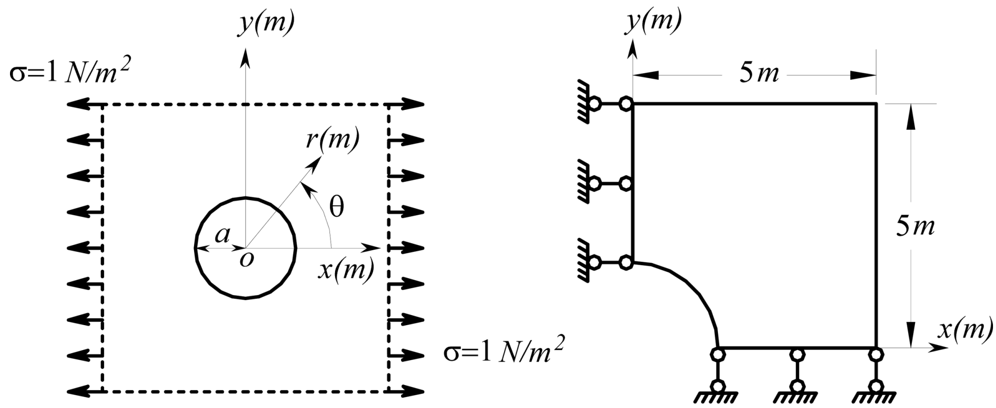

Fig. 7 Infinite plate with a circular hole subjected to unidirectional tension

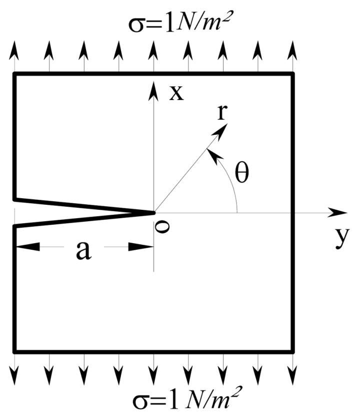

Fig. 8 Infinite plate with a crack subjected to unidirectional tension

For the cantilever problem, the exact displacements are given by Timoshenko and Goodier (1977) as

$$u_x = \frac{Py}{6EI}\left[(6L-3x)x + (2+\nu)\left(y^2 - \frac{1}{4}D^2\right)\right] \tag{32}$$

$$u_y = -\frac{P}{6EI}\left[3\,\nu y^2(L-x) + \frac{1}{4}D^2(4+5\,\nu)x + (3L-x)x^2\right] \tag{33}$$

and the stresses are

$$\sigma_{xx} = \frac{P(L-x)y}{I} \tag{34}$$

$$\sigma_{yy} = 0 \tag{35}$$

$$\sigma_{xy} = -\frac{P}{2I}\left(\frac{D^2}{4} - y^2\right) \tag{36}$$

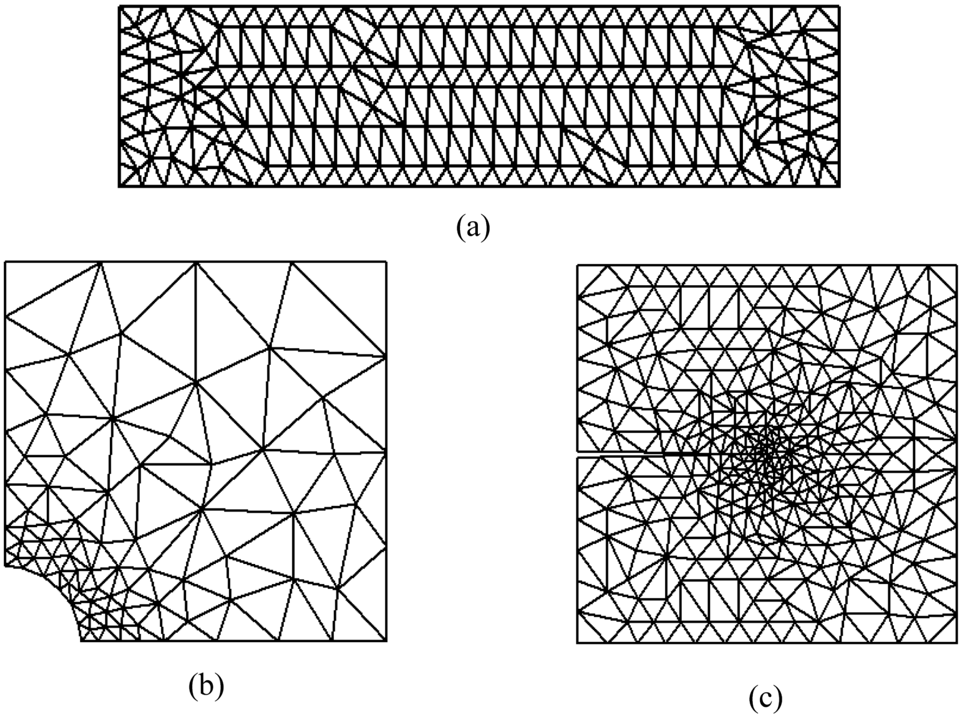

Fig. 9 Mesh model (a) cantilever (239 nodes), (b) infinite square plate with a hole (87 nodes) and (c) infinite square plate with a crack (344 nodes)

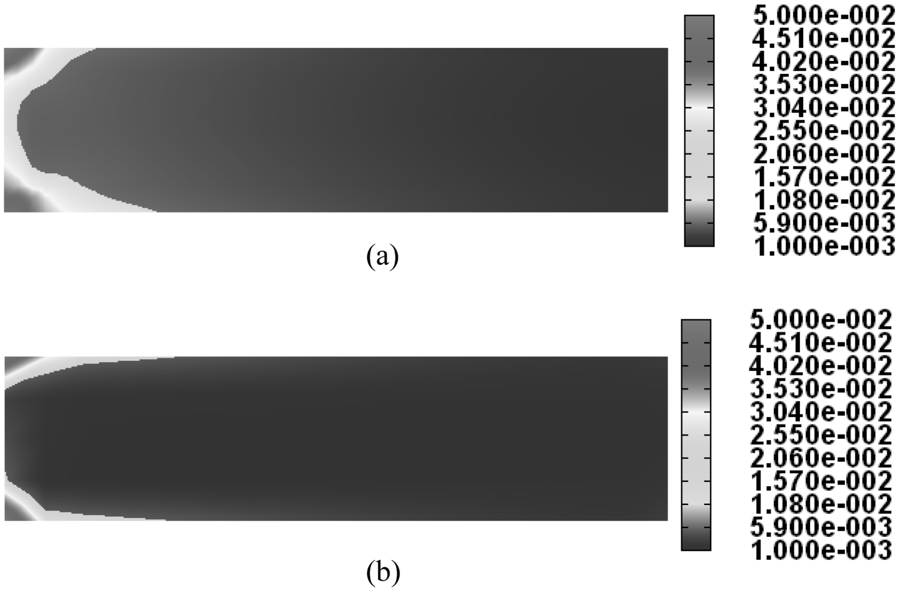

Fig. 10 Error distribution in the cantilever (a) distribution of estimated SDE error and (b) distribution of exact error

where

$$I = \frac{D^3}{12} \tag{37}$$

The parameters used are $D = 12$, $L = 48$ and $P = -1000$. The boundaries, $x = 0$ and $x = L$, are prescribed respectively by exact displacement and traction computed from Eq. (32). The mesh model (see Fig. 9(a)) comprises 239 nodes. The distribution of estimated energy error (see Fig. 10(a)) demonstrates a close agreement with that of the exact error (see Fig. 10(b)) that is integrated over the element using the exact analytical solution of stresses and strains. From these figures, it is clearly observed that for the region which needs to refine, i.e., the high error region, the distribution of estimated local error is almost identical with that of exact local error.

For the problem of infinite plate with a hole, the analytical stresses are (Timoshenko and Goodier 1977)

$$\sigma_{xx}(x,y) = 1 - \frac{a^2}{r^2}\left(\frac{3}{2}\cos 2\theta + \cos 4\theta\right) + \frac{3a^4}{2r^4}\cos 4\theta \tag{38}$$

$$\sigma_{yy}(x,y) = -\frac{a^2}{r^2}\left(\frac{1}{2}\cos 2\theta - \cos 4\theta\right) - \frac{3a^4}{2r^4}\cos 4\theta \tag{39}$$

$$\sigma_{xy}(x,y) = -\frac{a^2}{r^2}\left(\frac{1}{2}\sin 2\theta + \sin 4\theta\right) + \frac{3a^4}{2r^4}\sin 4\theta \tag{40}$$

where a is the radius of the hole and (r, θ) the polar coordinate of a point. In the computation, only one quarter of the domain is analyzed due to the dual symmetry, with all boundaries prescribed by exact solutions. The mesh model (87 nodes) and error distributions are shown in Figs. 9(b), 11(a) and 11(b) respectively. Again, the high error region distributions of the predicted and the exact error show a very good agreement.

In the crack-tip field problem, the square plate has a side of $2a$ and the crack assumes a length of a. This corresponds to the so-called Griffith mode-I crack problem which has an analytical solution (Anderson 1991)

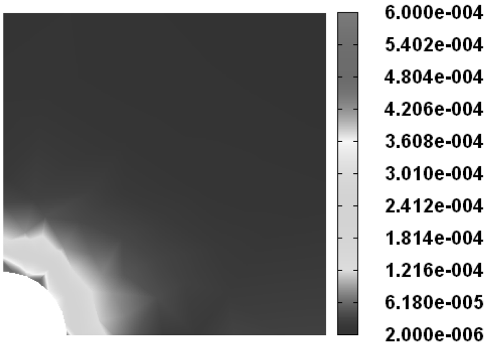

(a)

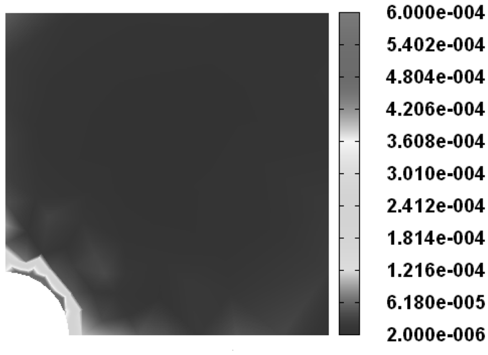

(b)

Fig. 11 Error distribution for square plate with a hole (a) distribution of estimated SDE error and (b) distribution of exact error

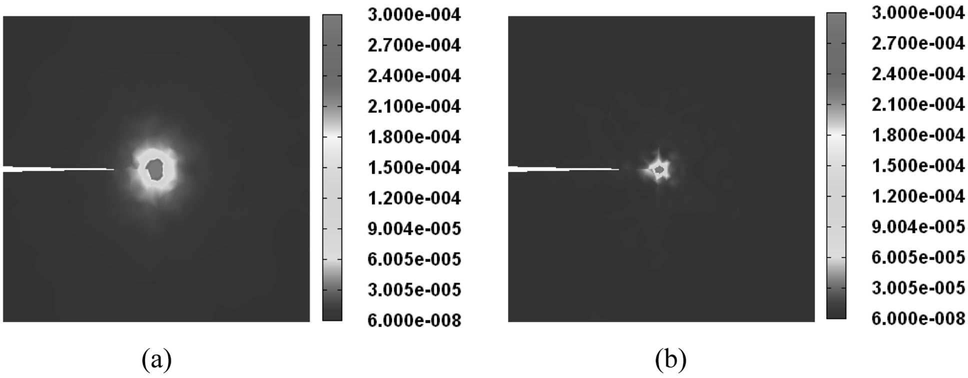

Fig. 12 Error distribution for square plate with a crack (a) distribution of estimated SDE error and (b) distribution of exact error

$$\sigma_{xx} = \frac{K_I}{\sqrt{2\pi r}}\cos\frac{\theta}{2}\left(1-\sin\frac{\theta}{2}\sin\frac{3\theta}{2}\right) \tag{41}$$

$$\sigma_{yy} = \frac{K_I}{\sqrt{2\pi r}}\cos\frac{\theta}{2}\left(1+\sin\frac{\theta}{2}\sin\frac{3\theta}{2}\right) \tag{42}$$

$$\sigma_{xy} = \frac{K_I}{\sqrt{2\pi r}}\sin\frac{\theta}{2}\cos\frac{\theta}{2}\cos\frac{3\theta}{2} \tag{43}$$

The coordinate system is depicted in Fig. 8. The stress intensity factor K_I is prescribed by $K_I = \sqrt{\pi a}$. In the mesh model, 344 nodes are used as shown in Fig. 9(c). Similar to the previous two examples, the stress concentration at the crack tip and high error region can be estimated properly by proposed local error estimate as shown in Fig. 12.

6.2 Local adaptive refinement

The performance of local adaptive refinement procedure is demonstrated in four typical examples.

6.2.1 Infinite plate with a circular hole

A benchmark problem, infinite plate with a circular hole shown in Fig. 7, is analyzed using our adaptive schemes. The geometry and boundary conditions have been given above. The problem is analyzed with allowable global error estimation $\eta_{threshold}$ = 0.008 and mesh refinement percentage $\alpha = 10$. The refinement process is plotted in Fig. 14. It is clearly seen that stress concentration occurs around the hole, and the mesh is automatically refined at these locations. The convergence of stain energy of our adaptive scheme is much higher than that of the uniform refinement scheme as shown in Fig. 15(a), which demonstrates the effectiveness of the present adaptive procedure. Fig. 15(b) shows the comparison of strain energy obtained using different numerical methods (ES-FEM, NS-FEM and FEM) with the same meshes at various adaptive stages. It is obvious that the strain energy of ES-FEM is the closest to the analytical solution in Eq. (32) compared to other methods with the same mesh. This finding is consistent with results given in Liu *et al.* (2008) and confirms our expectation that ES-FEM is the most suitable for the adaptive analysis for fast

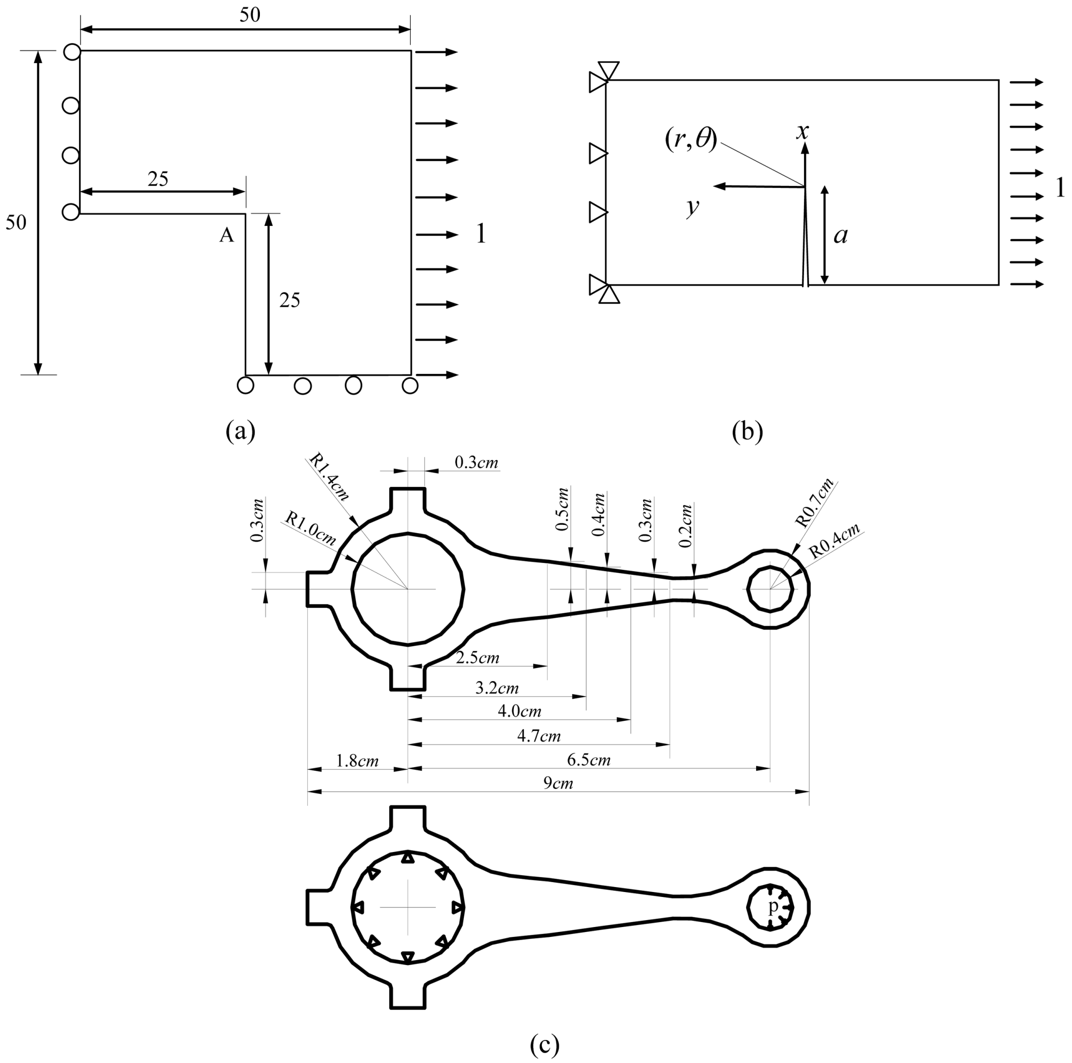

Fig. 13 Geometry model and boundary condition of (a) an L-shaped plate subjected to a unit horizontal tensile traction (b) a rectangular plate with a crack subjected to a unit tensile traction and (c) an automobile connecting bar

convergent results. We also note the fact that the NS-FEM gives an upper bound solution in strain energy to the exact solution, the FEM gives a lower bound solution, and the ES-FEM solution stays in between.

6.2.2 L-shaped plate

In this example, an L-shaped plate subjected to uniform tensile force in the horizontal direction as shown in Fig. 13(a) is analyzed. The plate is constrained in x and y directions along the left and bottom edges respectively. Plane stress problem is considered with the parameters $E = 3.0 \times 10^7$ Pa and $v = 0.3$. As the exact solution is not available, a reference solution is obtained using FEM with a very fine mesh (13667 nodes) for comparison.

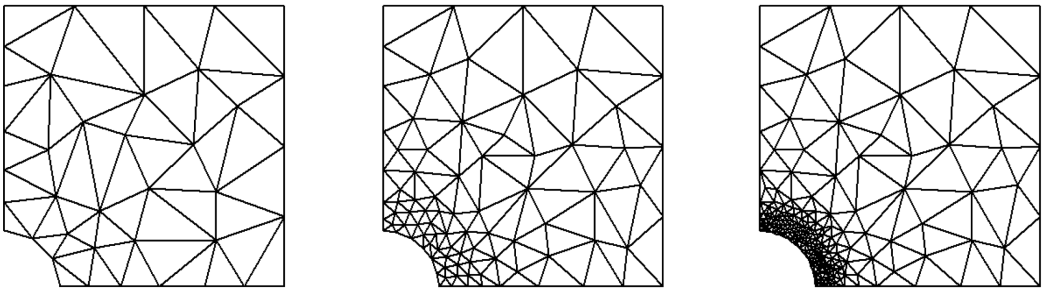

Step 1, 39 nodes Step 2, 87 nodes Step 3, 222 nodes

Fig. 14 The adaptive refinement stages for infinite square plate with a hole

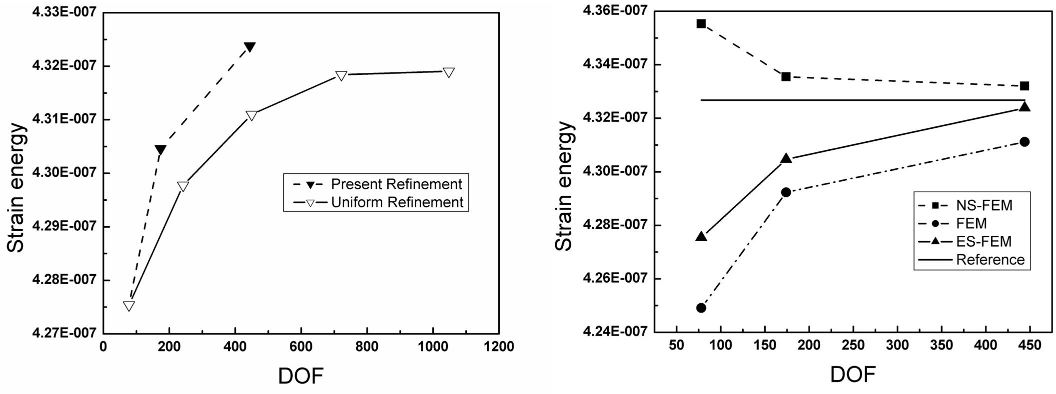

(a) (b)

Fig. 15 Infinite square plate with a hole (a) comparison of convergence process of solution in strain energy and (b) comparison of strain energy obtained using ES-FEM, NS-FEM and FEM with the same mesh

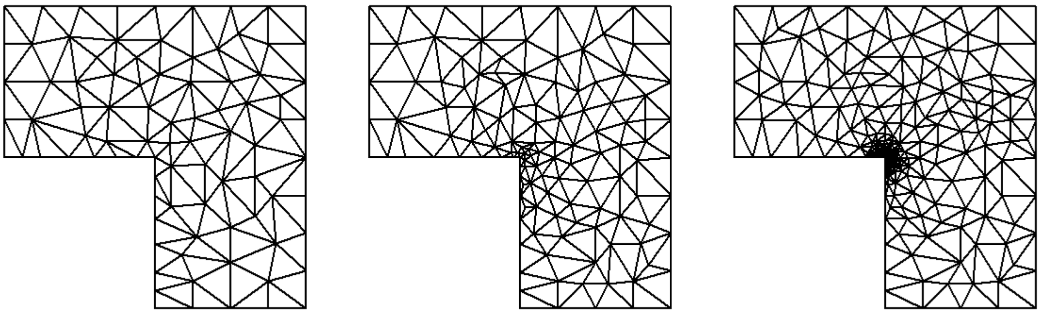

Step 1, 88 nodes Step 2, 127 nodes Step 3, 252 nodes

Fig. 16 The adaptive refinement stages for L shaped plate

During the adaptive analysis, controlling parameters $\eta_{threshold} = 0.02$ and $\alpha = 10$ are used. The refinement process take 3 steps and the mesh at these steps are shown in Fig. 16. It can be clearly seen that the refinement procedure detects automatically the singularity at the corner point and the mesh is automatically refined at the location around this point. The stress distribution obtained at

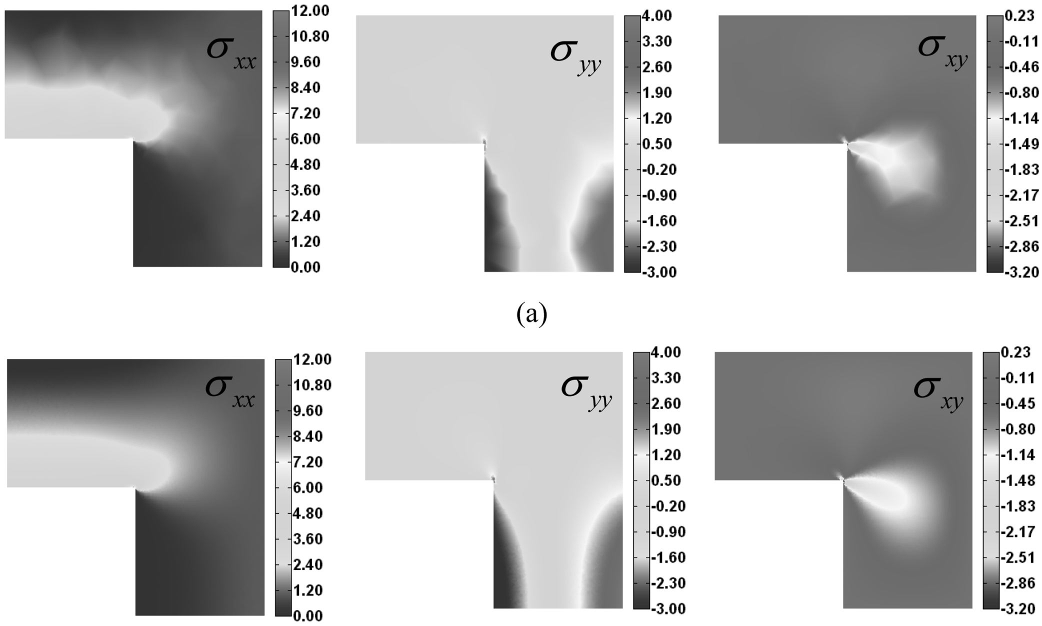

(b)

Fig. 17 The comparison of stress distributions for L shaped plate (a) solution at the final stage and (b) reference solution with 13667 nodes by FEM

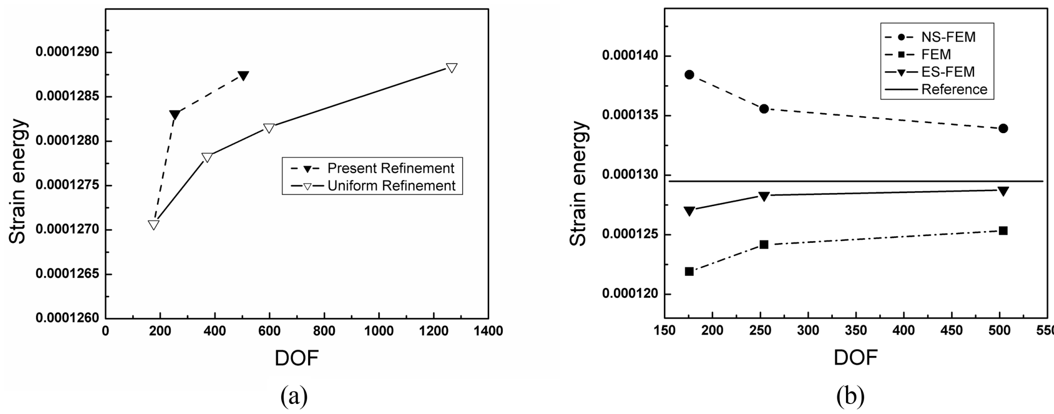

(a) (b)

Fig. 18 L shaped plate (a) comparison of convergence process of solution in strain energy and (b) comparison of strain energy obtained using ES-FEM, NS-FEM and FEM with the same mesh

the final step is very close to the reference solution (see Fig. 17(a) and Fig. 17(b)). Again, the convergence of stain energy of the present adaptive scheme is much faster than that of the uniform refinement as shown in Fig. 18(a) and the strain energy of ES-FEM is very close to reference solution at all states (see Fig. 18(b)). The superiority of ES-FEM in accuracy is obvious. We observed again that the NS-FEM gives an upper bound solution in strain energy to the exact solution, the FEM gives a lower bound solution, and the ES-FEM solution is in between.

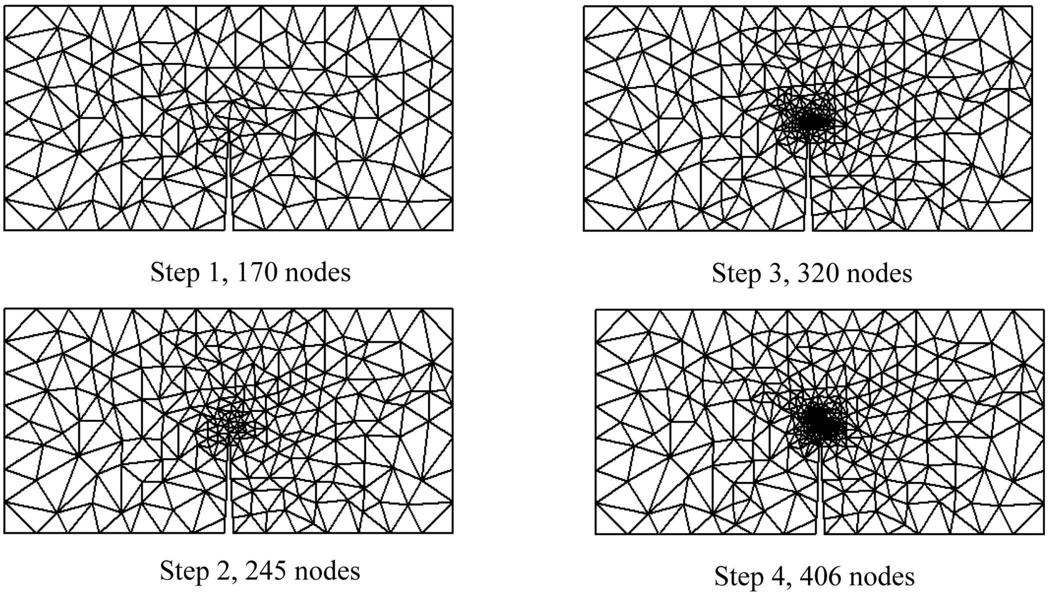

Fig. 19 The adaptive refinement stages for rectangular square plate with a crack

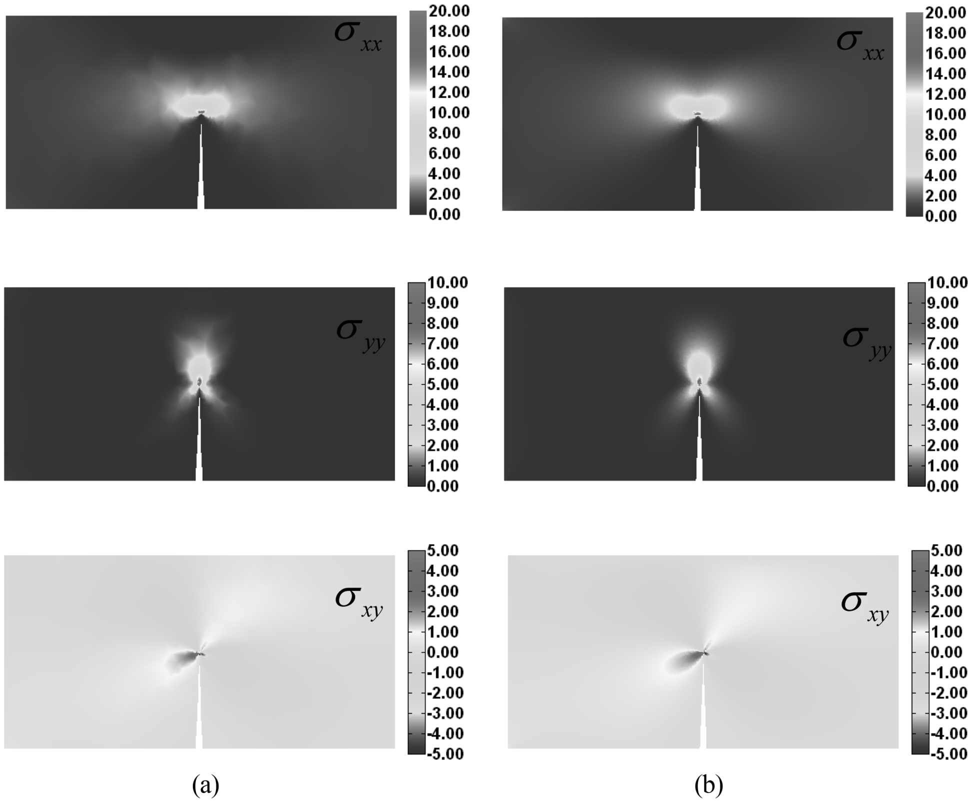

Fig. 20 The comparison of stress distributions for rectangular square plate with a crack (a) solution at the final stage and (b) reference solution with 13666 nodes by FEM

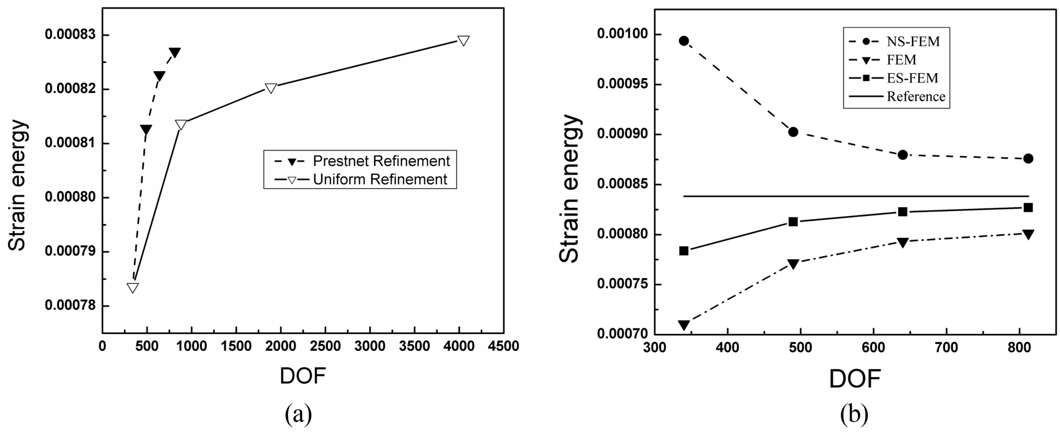

Fig. 21 Infinite square plate with a crack (a) comparison of convergence process of solution in strain energy and (b) comparison of strain energy obtained using ES-FEM, NS-FEM and FEM with the same mesh

6.2.3 Rectangular square plate with a crack

A rectangular square plate ($4a \times 2a$) with a crack of length a is considered, and the geometry model is shown in Fig. 13(b). The left edge of plate is constrained, while the right side is subjected horizontal unit traction. Plane stress problem is studied with the material parameters of E = 3.0×10^7 Pa and $v = 0.3$.

Adaptive analysis is implemented with parameters $\eta_{threshold} = 0.05$ and $\alpha = 5$. The refinement process takes 4 steps to complete, and the mesh at each stage is as shown in Fig. 19. It can be clearly observed that the refinement is performed mainly in the vicinity of crack tip. The stress distribution at the final step with 406 nodes is very close to the reference solution (see Fig. 20(a) and Fig. 20(b)), which is obtained using FEM with a very fine mesh (13666 nodes). As shown in Fig. 21, the convergence of stain energy of our adaptive scheme is always much faster than the uniform refinement process and ES-FEM obtains best accuracy compared to NS-FEM and FEM, which bound the solution from both sides.

6.2.4 An automotive part: connecting rod

Finally, a practical problem of typical connecting used in automobiles, as shown in Fig. 13(c), is studied using our adaptive code. The rod is constrained along the left circle and subjected to a uniform unit radial pressure along half of right circle as shown in the figure. The problem is considered as a plane stress problem with material parameters $E = 3.0 \times 10^7$ Pa and $v = 0.3$.

The problem is analyzed with $\eta_{threshold} = 0.05$ and $\alpha = 10$. The refinement process is plotted in Fig. 22(a). From the figure, stress concentration occurs around the vertical radius part of right pin hole and at the location with the transition of section, leading to an automatically refined mesh at these locations. The stress distribution at the final step shows a very good agreement with the reference solution (see Fig. 22(b) and Fig. 22(c)), which is obtained by using FEM with a very fine mesh of 16614 nodes. For this practical problem with complicated shape, the convergence of stain energy of our adaptive scheme is found again to converge much faster than the uniform refinement. The ES-FEM produces the most accurate result that together with the exact solution is bounded by the solutions of NS-FEM and FEM. These findings again demonstrate again that the proposed local adaptive refinement procedure based on ES-FEM is effective and efficient.

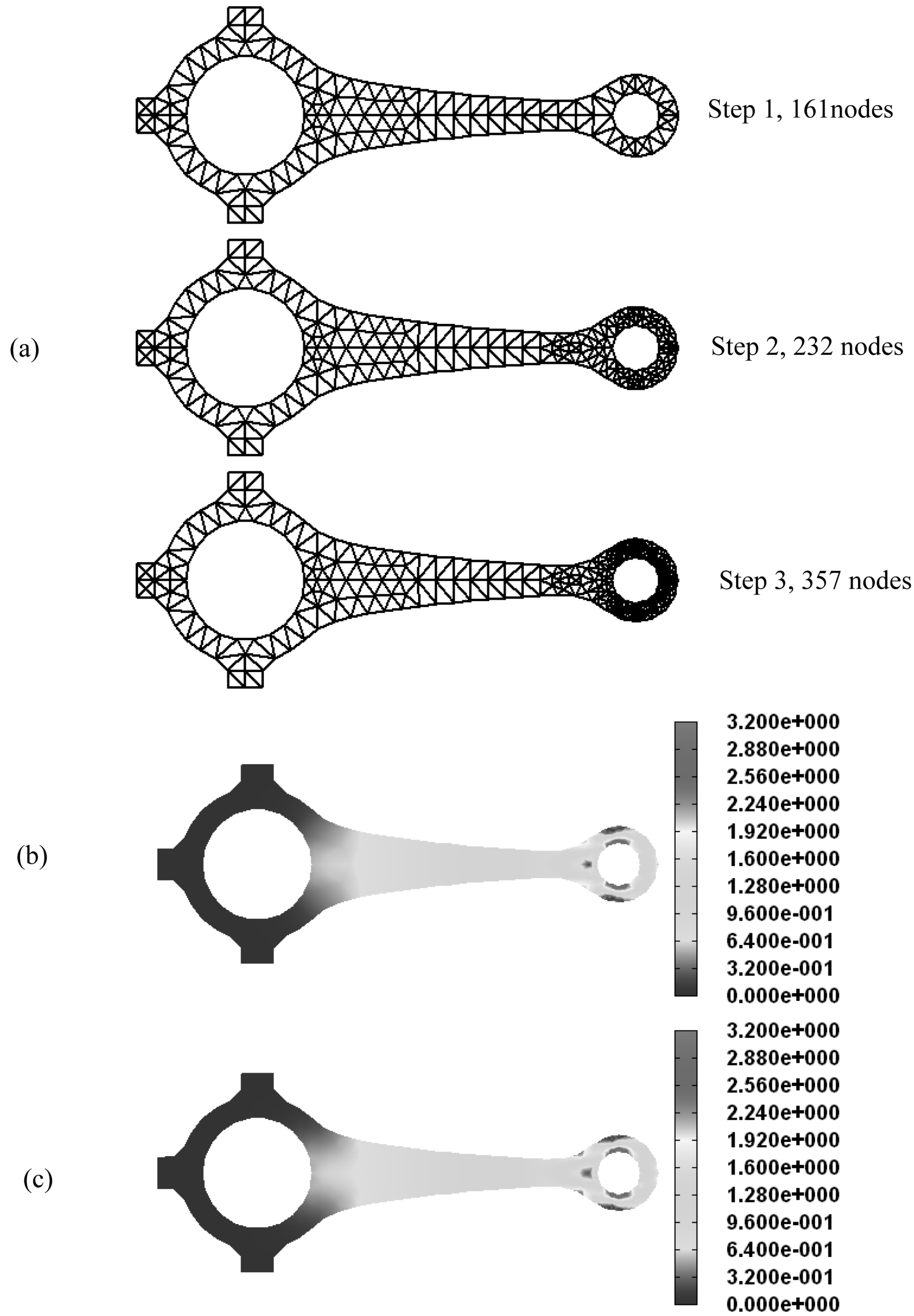

Fig. 22 The adaptive refinement process and comparison of stress distributions for connecting rod (a) 3 refinement stages; (b) von Mises stress distributions at the final stage and (c) reference von Mises stress distributions with 16614 nodes by FEM

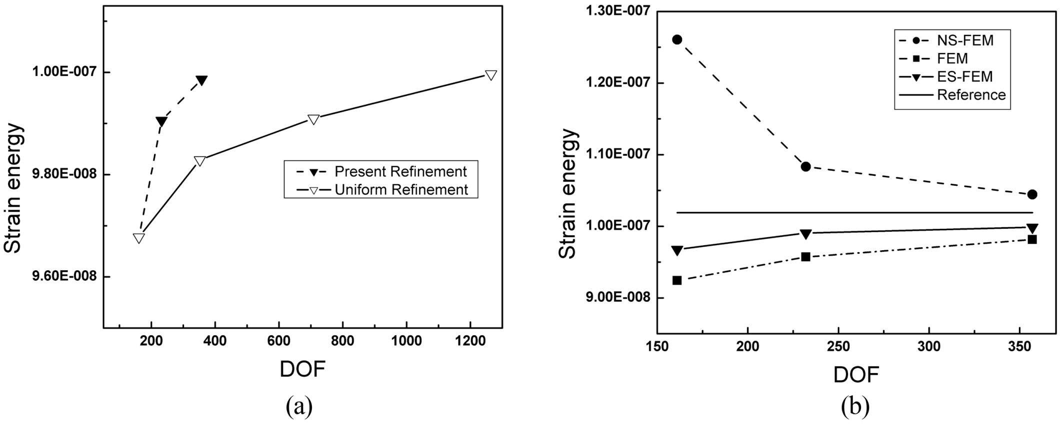

Fig. 23 Connecting rod (a) comparison of convergence process of solution in strain energy and (b) comparison of strain energy obtained using ES-FEM, NS-FEM and FEM with the same mesh

7. Conclusions

The complexity analysis of the edge-based smoothed finite element method (ES-FEM) using triangular elements is conducted in detail, and an efficient adaptive procedure is proposed for ES-FEM. The procedure consists of a smoothing domain based energy (SDE) error estimate and a local domain refinement technique. Through the formulation and numerical examples, some conclusions can be drawn as follows:

1. Taking the same renumbering strategy, the bandwidth of ES-FEM and NS-FEM is almost twice more than that of FEM. Therefore, the computation time is nearly 4 times more than that of FEM.
2. The SDE error estimate evaluates triangular element error based on the strain energy of maximum difference of strains among the three sub-smoothing domains associated with edges of elements. Numerical experiments have demonstrated that the proposed (SDE) error estimate is able to capture the high error region where needs to be refined.
3. A simple and efficient local domain refinement technique is developed using triangular mesh, which can be generated automatically and efficiently even for complicated domain with the aid of scaling factors. Refinement of a local domain is accomplished simply by adjusting a scaling factor, thus improving computational efficiency for practical problems.
4. The convergence of stain energy of our adaptive scheme is much higher than that of the uniform refinement, which demonstrates the effectiveness of the present adaptive procedure.
5. The NS-FEM gives an upper bound solution in strain energy to the exact solution, the FEM gives a lower bound solution, and the ES-FEM solution together with the exact solution is in between.

References

Anderson, T.L. (1991), *Fracture Mechanics: Fundamentals and Applications*, 1st Edition, CRC Press, Boca Raton.

Atluri, S.N. and Zhu, T.L. (1998), “A new meshless local Petrov-Galerkin (MLPG) approach in computational

mechanics", *Comput. Mech.*, **22**, 117-127.
Babuska, I. and Rheinboldt, W.C. (1978), "A posteriori error estimates for the finite element method", *Int. J. Numer. Meth. Eng.*, **12**, 1597-1615.
Belytschko, T., Lu, Y.Y. and Gu, L. (1994), "Element free Garlerkin methods", *Int. J. Numer. Meth. Eng.*, **37**, 229-256.
Chen, J.S., Wu, C.T. and Belytschko, T. (2000), "Regularization of material instabilities by meshfree approximations with intrinsic length scales", *Int. J. Numer. Meth. Eng.*, **47**, 1303-1322.
Chen, J.S., Wu, C.T., Yoon, S. and You, Y. (2001), "A stabilized conforming nodal integration for Galerkin mesh-free methods", *Int. J. Numer. Meth. Eng.*, **50**, 435-466.
Chung, H.J. and Belytschko, T. (1998), "An error estimate in the EFG method", *Comput. Mech.*, **21**, 91-100.
Choi, C.K. and Chung, H.J. (1995), "An adaptive-control of spatial-temporal discretization error in finite-element analysis of dynamic problems", *Struct. Eng. Mech.*, **3**, 391-410.
Dohrmann, C.R., Heinstein, M.W., Jung, J., Key, S.W. and Witkowski, W.R. (2000), "Node-based uniform strain elements for three-node triangular and four-node tetrahedral meshes", *Int. J. Numer. Meth. Eng.*, **47**, 1549-1568.
Eringen, A.C. and Edelen, D.G.B. (1972), "On nonlocal elasticity", *Int. J. Eng. Sci.*, **10**, 233-248.
Kee, B.B.T., Liu, G.R. and Zhang, G.Y. (2008), "A residual based error estimator using radial basis functions", *Finite Elem. Anal. Des.*, **44**, 631-645.
Lee, C., Im, C.H. and Jung, H.K. (1998), "A posteriori error estimation and adaptive node refinement for fast moving least square reproducing kernel (FMLSRK) method", *CMES: Comp. Model. Eng. Sci.*, **20**, 35-41.
Liu G.R. (2002), *Mesh Free Methods: Moving Beyond the Finite Element Method*, CRC Press, Boca Raton.
Liu, G.R. (2008), "A generalized gradient smoothing technique and the smoothed bilinear form for Galerkin formula of a wide class of computational methods", *Int. J. Comput. Meth.*, **5**, 199-236.
Liu, G.R., Dai, K.Y. and Nguyen, T.T. (2007), "A smoothed finite element method for mechanics problems", *Comput. Mech.*, **39**, 859-877.
Liu, G.R., Nguyen, T.T. and Dai, K.Y. (2007), "Theoretical aspects of the smoothed finite element method (SFEM)", *Int. J. Numer. Meth. Eng.*, **71**, 902-930.
Liu, G.R., Nguyen-Thoi, T. and Lam, K.Y. (2008), "An edge-based smoothed finite element method (ES-FEM) for static, free and forced vibration analysis", *J. Sound Vib.*, **320**, 1100-1130.
Liu, G.R., Nguyen-Thoi, T. and Lam, K.Y. (2009), "A node-based smoothed finite element method for upper bound solution to solid problems (NS-FEM)", *Comput. Struct.*, **87**, 14-26.
Liu, G.R., Nguyen-Thoi, T., Nguyen-Xuan, H., Dai, K.Y. and Lam, K.Y. (2009), "On the essence and the evaluation of the shape functions for the smoothed finite element method (SFEM)", *Int. J. Numer. Meth. Eng.*, **77**, 1863-1869.
Liu, G.R. and Quek, S.S. (2003), *The Finite Element Method: A Practical Course*, Butterworth Heinemann, Oxford.
Liu, G.R. and Tu, Z.H. (2002), "An adaptive procedure based on background cells for Meshfree methods", *Comput. Meth. Appl. Mech. Eng.,* **191**, 1923-1943.
Liu, G.R. and Zhang, G.Y. (2005), "A linearly conforming point interpolation method (LC-PIM) for 2D solid mechanics problems", *Int. J. Comput. Meth.*, **2**, 645-665.
Lucy, L.B. (1977), "Numerical approach to testing the fission hypothesis", *Astrono. J.*, **82**, 1013-1024.
Nguyen-Thoi, T., Liu, G.R. and Lam, K.Y. (2009), "A face-based smoothed finite element method (FS-FEM) for 3D linear and nonlinear solid mechanics problems using 4-node tetrahedral elements", *Int. J. Numer. Meth. Eng.*, **78**, 324-353.
Ozakca, M. (2003), "Comparison of error estimation methods and adaptivity for plane stress/strain problems", *Struct. Eng. Mech.*, **15**, 579-608.
Timoshenko, S.P. and Goodier, J.N. (1977), *Theory of Elasticity*, McGraw-Hill, New York.
Yoo, J., Moran, W.B. and Chen, J.S. (2004), "Stabilized conforming nodal integration in the natural-element method", *Int. J. Numer. Meth. Eng.*, **60**, 861-890.
Zhang, G.Y. and Liu, G.R. (2008), "An efficient adaptive analysis procedure for certified solutions with exact bounds of strain energy for elastic problems", *Finite Elem. Anal. Des.*, **44**, 831-841.
Zhang, J., Liu, G.R., Lam, K.Y., Li, H. and Xu, G. (2008), "A gradient smoothing method (GSM) based on

strong form governing equation for adaptive analysis of solid mechanics problems", *Finite Elem. Anal. Des*., **44**, 889-909.

Zienkiewicz, O.C. and Taylor, R.L. (2000), *The Finite Element Method,* 5th Edition, Butterworth Heinemann, Oxford.

Zienkiewicz, O.C. and Zhu, J.Z. (1987), "A simple error estimator and adaptive procedure for practical engineering analysis", *Int. J. Numer. Meth. Eng*., **24**, 337-357.